Anisotropic H_{c2} up to 92 T and the signature of multiband superconductivity in $Ca_{10}(Pt_4As_8)((Fe_{1-x}Pt_x)_2As_2)_5$

Eundeok Mun,[1] Ni Ni,[2] Jared M. Allred,[2] Robert J. Cava,[2] Oscar Ayala,[1] Ross D. McDonald,[1]
Neil Harrison,[1] and Vivien S. Zapf[1]

[1]*National High Magnetic Field Laboratory, Los Alamos National Laboratory, Los Alamos, New Mexico 87545, USA*
[2]*Department of Chemistry, Princeton University, Princeton, New Jersey 08544, USA*

The upper critical fields $H_{c2}(T)$ of single crystals of the superconductor $Ca_{10}(Pt_{4-\delta}As_8)((Fe_{0.97}Pt_{0.03})_2As_2)_5$ ($\delta \approx 0.246$) are determined over a wide range of temperatures down to $T = 1.42$ K and magnetic fields of up to $\mu_0 H \simeq 92$ T. The measurements of anisotropic $H_{c2}(T)$ curves are performed in pulsed magnetic fields using radio-frequency contactless penetration depth measurements for magnetic field applied both parallel and perpendicular to the **ab** plane. Whereas a clear upward curvature in $H_{c2}^{\|\mathbf{c}}(T)$ along $\mathbf{H} \| \mathbf{c}$ is observed with decreasing temperature, the $H_{c2}^{\|\mathbf{ab}}(T)$ along $\mathbf{H} \| \mathbf{ab}$ shows a flattening at low temperatures. The rapid increase of the $H_{c2}^{\|\mathbf{c}}(T)$ at low temperatures suggests that the superconductivity can be described by two dominating bands. The anisotropy parameter $\gamma_H \equiv H_{c2}^{\|\mathbf{ab}}/H_{c2}^{\|\mathbf{c}}$ is ~ 7 close to T_c and decreases considerably to ~ 1 with decreasing temperature, showing rather weak anisotropy at low temperatures.

After the discovery of superconductivity in the $LaFeAsO_{1-x}F_x$ system, enormous research efforts have been devoted to searching for Fe-based superconductors with higher transition temperatures T_c, and they have been discovered and categorized into several types.[1–6] All of these materials have layers with edge-sharing tetrahedra, where Fe atoms are surrounded by four As or Se atoms. Recently, $Ca_{10}(Pt_nAs_8)(Fe_2As_2)_5$ systems have shown that the T_c can be as high as ~ 38 K by substituting Pt for Fe in the Fe_2As_2 layer.[7–9] These structures have stacks of Ca-(Pt_nAs_8)-Ca-(Fe_2As_2), forming a triclinic $P\bar{1}$, 10-3-8 phase with $n = 3$ and tetragonal $P4/n$, 10-4-8 phase with $n = 4$.[7]

Upper critical field H_{c2} measurements of many Fe-based superconductors have revealed similar temperature dependences of the anisotropy ratio $\gamma_H \equiv H_{c2}^{\|\mathbf{ab}}/H_{c2}^{\|\mathbf{c}}$, decreasing with decreasing temperature, with $\gamma_H \lesssim 10$ close to the T_c.[10–17] As evidenced by both experiments and band-structure calculations, the Fe-based superconductors are a multiband system.[10–13,19–21] Multiband superconductivity can be manifested in the temperature dependence of the anisotropic parameters. For example, γ_H of MgB_2 decreases with increasing temperature,[22] whereas for many Fe-based materials, γ_H increases on warming.[10,13] For one-band isotropic materials, the anisotropic parameters generally have no temperature dependence.

In light of the multiband superconductivity and the very high $H_{c2}(0)$ of Fe-based superconductors, rapidly exceeding the limit of the commonly available magnetic fields, finding the true behavior of the $H_{c2}(T)$ and γ_H down to very low temperatures and high magnetic fields are of great interest. In this Rapid Communication, we present $H_{c2}(T)$ curves determined from radio-frequency (rf) contactless penetration depth measurements in pulsed magnetic fields up to 92 T, for single crystals of the 10-4-8 phase materials. The high magnetic fields up to 92 T and temperatures down to 1.42 K, used in this study, enable access to the complete evolution of the $H_{c2}(T)$ curves. We find that as the temperature decreases,

the $H_{c2}^{\|\mathbf{ab}}(T)$ curve flattens, whereas $H_{c2}^{\|\mathbf{c}}(T)$ increases steeply, which is shown to be consistent with the multiband effects.

The $Ca_{10}(Pt_{4-\delta}As_8)((Fe_{0.97}Pt_{0.03})_2As_2)_5$ ($\delta \approx 0.246$) samples with $T_c = 26.5$ K were prepared by heating precursor materials above $1100\,^\circ$C. The shape of the as-grown crystal is platelike in the **ab** plane with shiny surfaces. Details of sample growth and characterization are given in Ref. 7. To study the anisotropy of H_{c2} up to $\mu_0 H = 92$ T, the magnetic field dependence of rf contactless penetration depth, known as proximity detection oscillator (PDO),[23] was measured for magnetic field applied both parallel ($\mathbf{H} \| \mathbf{ab}$) and perpendicular ($\mathbf{H} \| \mathbf{c}$) to the **ab** plane of the tetragonal structure in two different pulsed magnet systems. The rf technique has been shown to be a sensitive and accurate method for determining the H_{c2} of superconductors, especially in pulsed magnetic fields.[24] Details about this technique can be found in Refs. 14, 17, and 23–25. For magnetic fields up to 60 T, a short-pulse magnet was used with a 10-ms rising and 40-ms falling time. Measurements were extended to 92 T in the 95 T multishot magnet system at the National High Magnetic Field Laboratory Pulsed Field Facility: Here, the magnetic fields up to ~ 36 T are provided by a motor-generator-driven outsert magnet with a slower sweep rate and longer pulse length (~ 2.5 s) and the remaining magnetic field from ~ 36 T up to 92 T is provided (within 15 ms) by a capacitor-bank-driven insert magnet. The magnetic field versus time profile of the insert magnet is shown in the inset to Fig. 1. Examples of resonance frequency shift (ΔF) measured using the rf technique are shown in Fig. 1, where changes in the resistivity and magnetic susceptibility drive a shift in the resonance frequency of an oscillator circuit. At ~ 36 T, ΔF shows a feature due to the rapid shift in the rate of change of magnetic field, as indicated by the vertical line in Fig. 1. The magnetic field was determined using a pick-up coil and calibrated by measuring quantum oscillations in copper. To minimize the eddy current heating and dissipative vortex motion due to the fast sweep rate of pulsed magnetic fields, small single crystals were chosen,
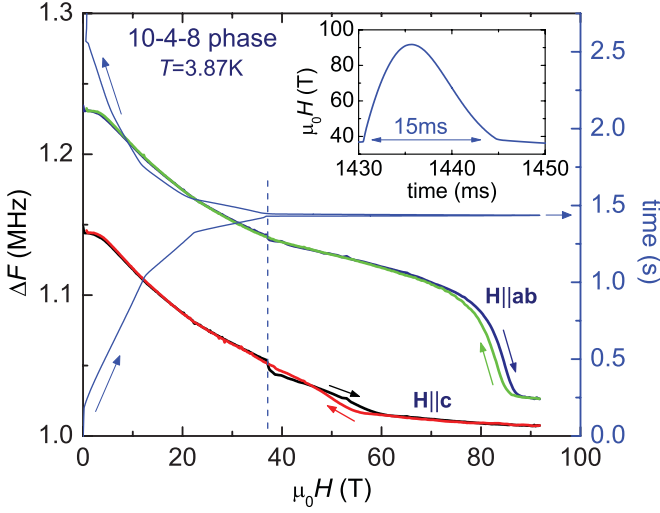
FIG. 1. (Color online) The representative data sets taken in a multishot magnet. Left axis: The rf frequency shift ΔF as a function of magnetic field for $\mathbf{H} \parallel \mathbf{ab}$ and $\mathbf{H} \parallel \mathbf{c}$ at $T = 3.87$ K. Right axis: The waveform of pulse for the 92 T. The fast sweep rate of magnetic fields up to 92 T (within 15 ms, see inset) is provided by a capacitor bank on the peak of the slowly sweeping $\sim$36 T magnetic field ($\sim$2.5 s) derived by a motor generator. Because of the radical change of magnetic field at $\sim$36 T, ΔF curves show a slope break, as indicated by the vertical dashed line.

typically $\sim 0.2 \times 0.2 \times 0.05$ mm^3. Note that in order to reduce open-loop area of samples for $\mathbf{H} \parallel \mathbf{c}$, a smaller size sample ($\sim 0.12 \times 0.12 \times 0.05$ mm^3) was used for measurements up to 92 T in the multishot magnet. No significant difference between 60 and 92 T measurements was detected.

In zero field, the superconducting transition temperature, determined from the $(d\Delta F)/dT$ analysis, gives $T_c = 26.5$ K for three samples, used in the both short-pulse 60 T and multishot 95 T magnet [inset in Fig. 2(a)]; as the temperature decreases, ΔF sharply increases at T_c. The evolution of superconductivity with magnetic field is shown in Fig. 2(a) for $\mathbf{H} \parallel \mathbf{ab}$ and Fig. 2(b) for $\mathbf{H} \parallel \mathbf{c}$. At this point, it should be noted that the phase transitions determined by the rf technique are consistent with offset criteria of resistance measurements shown in Ref. 17. In comparison with the samples reported in Ref. 7, samples studied in this work show a slightly higher T_c, related to the different Pt doping concentration in the Fe$_2$As$_2$ layer.

Using the deviation from the normal-state criterion, discussed in Ref. 17, the $H_{c2}(T)$ curve is inferred from the ΔF versus H plots shown in Figs. 2(a) and 2(b); the determined H_{c2} is indicated by arrows. Note that the H_{c2} error bar is estimated by the difference between the H_{c2} values determined by the point deviating from the background and by taking the slope of the rf signal intercepting the slope of the normal-state background.[17] In addition, the hysteresis detected in 92 T multishot measurements (see Fig. 1) is considered to determine the error bar. The obtained $H_{c2}(T)$ curves for both $\mathbf{H} \parallel \mathbf{ab}$ and $\mathbf{H} \parallel \mathbf{c}$ are plotted in Fig. 3, as determined from the $H < 60$ T in a short pulse (squares) and from the $H < 92$ T in a multishot (circles) taken from the down-sweep of the magnetic field. The star symbols in Fig. 3 are extracted by linear extrapolation of
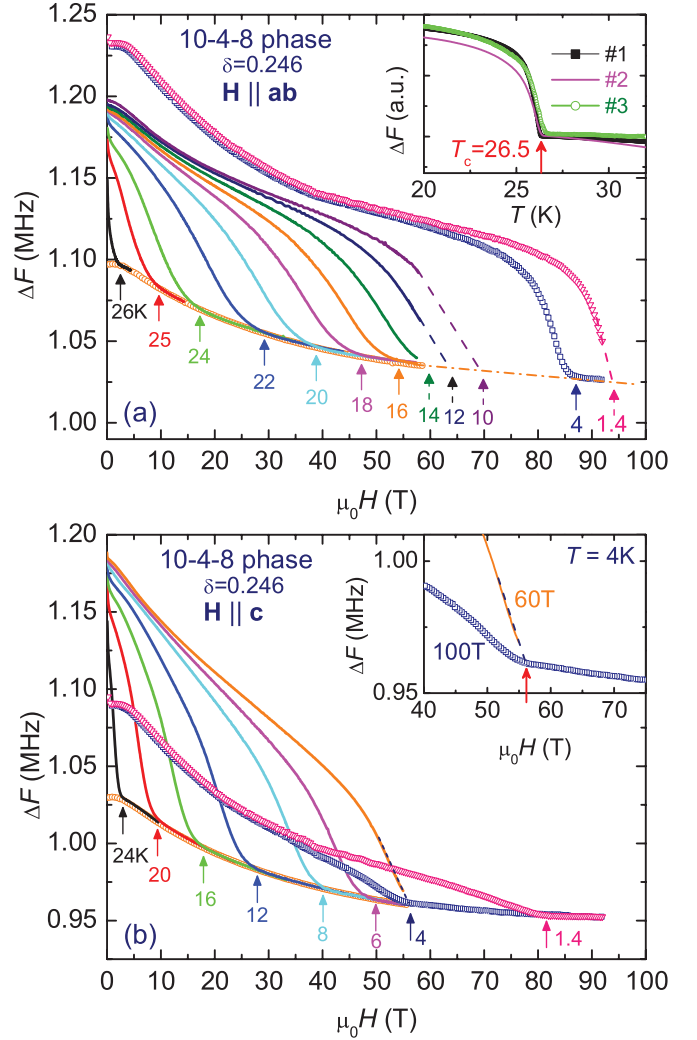

FIG. 2. (Color online) (a) ΔF as a function of magnetic field for $\mathbf{H} \parallel \mathbf{ab}$ at selected temperatures. Solid lines are 60 T short-pulse measurements and symbols (triangle and square) are 92 T multishot measurements. Open circles are ΔF taken at 28 K as a normal-state background signal. The determined H_{c2} is indicated by arrows. The dashed lines represent the linear extrapolation of ΔF to the normal state. The horizontal dashed-dotted line is a guide to the eye. The inset shows the temperature dependence of ΔF at $H = 0$ for three samples. (b) ΔF as a function of magnetic field for $\mathbf{H} \parallel \mathbf{c}$ at selected temperatures. Due to the small size of the sample used, the ΔF measured in the multishot magnet is small compared to the 60 T curve. Inset shows ΔF curves at $T = 4$ K from both magnet systems. The arrow indicates the H_{c2} determined by the 92 T measurement.

ΔF curves at $H < 60$ T and $H < 92$ T, as shown by dashed lines in Figs. 2(a) and 2(b). As a representative curve, ΔF taken at 4 K in a 60-T short-pulse magnet is presented in the inset of Fig. 2(b), where the critical field determined by extrapolating ΔF curve is consistent with the one determined by down-sweep of the 92 T magnetic field. The shapes of the $H_{c2}(T)$ curves for $\mathbf{H} \parallel \mathbf{ab}$ and $\mathbf{H} \parallel \mathbf{c}$ in Fig. 3 clearly show the different temperature dependence. A conventional linear field dependence of H_{c2} is observed close to the T_c, with clearly different slopes for the two field orientations. In the low-field
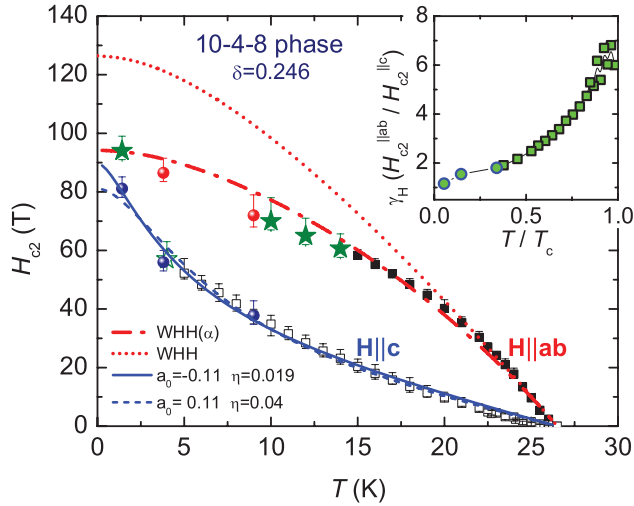
FIG. 3. (Color online) Anisotropic $H_{c2}(T)$ for 10-4-8 phase single crystals. The square symbols are obtained from the 60 T short pulse and circles are taken from the 95 T multishot magnet. The star symbols are extracted by the linear extrapolation of ΔF, as shown by dashed lines in Figs. 2(a) and 2(b). For $\mathbf{H} \parallel \mathbf{ab}$, the dotted line is the WHH H_{c2} and the dashed-dotted line represents the fit with $H_{c2}^* = H_{c2}/\sqrt{1+\alpha^2}$ ($\alpha \approx 0.9$). For $\mathbf{H} \parallel \mathbf{c}$, the solid line is a best fit of the two-band model to the experimental data with $a_0 = -0.11$ and $\eta = 0.019$ and the dashed line represents the fit with a fixed value of $a_0 = 0.11$. Inset shows the temperature dependence of the anisotropy $\gamma_H \equiv H_{c2}^{\parallel ab}/H_{c2}^{\parallel c}$. Squares and circles are determined from H_{c2} taken in the 60 T short pulse and 95 T multishot magnet, respectively.

region, the H_{c2} curves are consistent with earlier resistance study.[7] Toward higher fields, $H_{c2}^{\parallel ab}$ presents a tendency to saturate, whereas the curve for $H_{c2}^{\parallel c}$ shows a steep increase.

The anisotropy coefficient γ_H is plotted in the inset of Fig. 3. One can see that the value of γ_H is ~ 7 near T_c and then decreases considerably to ~ 1 with decreasing temperature. This temperature dependence of γ_H is similar to other Fe-based superconductors. Close to T_c, the γ_H of the 10-4-8 phase is bigger than that of the 122 type[13–15] and is comparable to the 1111 type.[10,11] Based on the results measured here and in other studies, this temperature dependence of γ_H and a weak anisotropy at $T \ll T_c$ seem to be a general feature of the Fe-based superconductors. The strong temperature dependence of γ_H can be a signature of multiband superconductivity. Based on the recent literature,[26] however, the γ_H can even have a weak temperature dependence for a single-band d-wave order parameter. Thus, our γ_H results need to be carefully analyzed.

The zero-temperature limit of H_{c2} can be predicted by using the Werthamer-Helfand-Hohenberg (WHH) theory,[27] which gives $H_{c2} = 0.69 T_c (dH_{c2}/dT)|_{T_c}$. The values of $H_{c2}(0)$ for $\mathbf{H} \parallel \mathbf{ab}$ and $\mathbf{H} \perp \mathbf{c}$ are estimated to be $H_{c2}^{\parallel ab} \sim 132$ T and $H_{c2}^{\parallel c} \sim 24$ T, respectively. For $T < 0.6\, T_c$, the $H_{c2}^{\parallel ab}$ already exceeds the Pauli limit ($H_p = 1.84\, T_c$),[28] giving $H_P \sim 48.7$ T. Clearly, these values do not capture the salient physics of this compound.

A number of experimental and theoretical papers have discussed the Fe-based superconductors as a two-band system.[10–13,19–21] Certainly, multiband superconductivity can be manifested in the $H_{c2}(T)$ curve, as shown in MgB$_2$.[22]

The clear upward curvature in $H_{c2}^{\parallel c}$ in the 10-4-8 phase can not be explained by the one-gap WHH theory and, therefore, suggests the multiband nature of superconductivity. In the dirty limit, the two-band model for H_{c2},[22] which takes into account both orbital and Zeeman pair breaking for negligible interband scattering, is thus used to fit the data so that a qualitative understanding can be reached. Assuming negligible interband scattering, the equation of $H_{c2}(T)$ can be written as $a_0[\ln t + U(h/t)][\ln t + U(\eta h/t)] + a_2[\ln t + U(\eta h/t)] + a_1[\ln t + U(h/t)] = 0$, where $a_0 = 2(\lambda_{11}\lambda_{22} - \lambda_{12}\lambda_{21})$, $a_1 = 1 + (\lambda_{11} - \lambda_{22})/\lambda_0$, $a_2 = 1 - (\lambda_{11} - \lambda_{22})/\lambda_0$, $\lambda_0 = [(\lambda_{11} - \lambda_{22})^2 + 4\lambda_{12}\lambda_{21}]^{1/2}$, $h = H_{c2}D_1/2\phi_0 T$, $t = T/T_c$, $\eta = D_2/D_1$, and $U(x) = \psi(x + 1/2) - \psi(x)$. $\psi(x)$ is the digamma function, λ_{11} and λ_{22} are the intraband BCS coupling constants, while λ_{12} and λ_{21} are the interband BCS coupling constants, and D_1 and D_2 are the in-plane diffusivity of each band.

As can be inferred from the equation, if $a_0 > 0$, the intraband coupling dominates, while if $a_0 < 0$, the interband coupling dominates. We assume $\lambda_{11} = \lambda_{22}$, such that $a_1 = a_2 = 1$, so that the shape of the curve is only determined by fitting parameters a_0 and η. The best-fit $H_{c2}^{\parallel c}$ curve with $a_0 = -0.11$ and $\eta = 0.019$ is shown as a solid blue line in Fig. 3, and can be seen to agree very well with the experimental data. Although $a_0 < 0$ for the best fit, it can not be concluded that the interband coupling dominates. The dashed blue curve, obtained by a fixed $a_0 = 0.11$ (intraband coupling dominates), also fits the data if the error bars are considered. The small η implies stronger scattering in one of the bands. Although the exact determination of the band coupling is not possible from our data analysis, the H_{c2} curvature for $H_{c2}^{\parallel c}$ can be explained well by the two-band model.

For $H_{c2}^{\parallel c}$, the orbital limit is comparable to the Pauli limit and the two-band model works well. For $H_{c2}^{\parallel ab}$, however, the two-band model fit does not result in physically meaningful parameters since the orbital limit is much larger than the Pauli limit. When including Pauli paramagnetism, the $H_{c2}^{\parallel ab}(T)$ curve can be fit with $H_{c2}^* = H_{c2}/\sqrt{1+\alpha^2}$, where the Maki parameter $\alpha = \sqrt{2}H_{c2}/H_P$.[29] A rather good agreement between the data and fitting is observed as shown by the dashed-dotted red line in Fig. 3.

An interesting behavior in the H_{c2} curves for the 10-4-8 phase is that the $\mathbf{H} \parallel \mathbf{ab}$ and $\mathbf{H} \parallel \mathbf{c}$ curves as seen to merge at low temperatures ($\gamma_H \sim 1$). For optimally Co-doped BaFe$_2$As$_2$,[13] the H_{c2} curves for the two field orientations also appear to meet at $T = 0$ K. The Te-doped FeSe system[16] shows crossing H_{c2} curves between $\mathbf{H} \parallel \mathbf{ab}$ and $\mathbf{H} \parallel \mathbf{c}$ because of the subsequent flattening of the $H_{c2}^{\parallel ab}$ curve at low temperatures. However, the H_{c2} curves in Co-doped BaFe$_2$As$_2$,[15] K$_{0.8}$Fe$_{1.76}$Se$_2$,[17] LiFeAs,[18] and oxypnictide systems[10–12] do not show such a crossing behavior.

In summary, we have determined the upper critical fields $H_{c2}(T)$ of the Ca$_{10}$(Pt$_{4-\delta}$As$_8$)((Fe$_{0.97}$Pt$_{0.03}$)$_2$As$_2$)$_5$ ($\delta \approx 0.246$) superconductor by measuring the rf contactless penetration depth up to 92 T in pulsed magnetic fields, which enable access to the complete evolution of $H_{c2}(T)$ curves. It was found that this superconductor shows very high $H_{c2}(0)$ values (~ 90 T for $\mathbf{H} \parallel \mathbf{c}$ and ~ 94 T for $\mathbf{H} \parallel \mathbf{ab}$) and relatively weak anisotropy

of superconductivity at low temperatures. For $\mathbf{H} \parallel \mathbf{ab}$, $H_{c2}(T)$ can be described by taking into account Pauli paramagnetism, whereas for $\mathbf{H} \parallel \mathbf{c}$, $H_{c2}(T)$ exhibits a steep increase at low temperatures, quite possibly due to the multiband effect.

[1] Y. Kamihara, T. Watanabe, M. Hirano, and H. Hosono, J. Am. Chem. Soc. **130**, 3296 (2008).

[2] F. C. Hsu, J. Y. Luo, K. W. Yeh, T. K. Chen, T. W. Huang, P. M. Wu, Y. C. Lee, Y. L. Huang, Y. Y. Chu, D. C. Yan, and M. K. Wu, Proc. Natl. Acad. Sci. USA **105**, 14262 (2008).

[3] M. Rotter, M. Tegel, and D. Johrendt, Phys. Rev. Lett. **101**, 107006 (2008).

[4] M. J. Pitcher, D. R. Parker, P. Adamson, S. J. C. Herkelrath, A. T. Boothroyd, and S. J. Clarke, Chem. Commun. (Cambridge) **45**, 5918 (2008).

[5] D. R. Parker, M. J. Pitcher, P. J. Baker, I. Franke, T. Lancaster, S. J. Blundell, and S. J. Clarke, Chem. Commun. 2189 (2009).

[6] J. Guo, S. Jin, G. Wang, S. Wang, K. Zhu, T. Zhou, M. He, and X. Chen, Phys. Rev. B **82**, 180520 (2010).

[7] N. Ni, J. M. Allred, B. C. Chan, and R. J. Cava, Proc. Natl. Acad. Sci. USA **108**, E1019 (2011).

[8] S. Kakiya, K. Kudo, Y. Nishikubo, K. Oku, E. Nishibori, H. Sawa, T. Yamamoto, T. Nozaka, and M. Nohara, J. Phys. Soc. Jpn. **80**, 093704 (2011).

[9] C. Löhnert, T. Stürzer, M. Tegel, R. Frankovsky, G. Friederichs, and D. Johrendt, Angew. Chem. Int. Ed. **50**, 9195 (2011).

[10] F. Hunte, J. Jaroszynski, A. Gurevich, D. C. Larbalestier, R. Jin, A. S. Sefat, M. A. McGuire, B. C. Sales, D. K. Christen, and D. Mandrus, Nature (London) **453**, 903 (2008).

[11] J. Jaroszynski, F. Hunte, L. Balicas, Y.-J. Jo, I. Raičević, A. Gurevich, D. C. Larbalestier, F. F. Balakirev, L. Fang, P. Cheng, Y. Jia, and H.-H. Wen, Phys. Rev. B **78**, 174523 (2008).

[12] H. S. Lee, M. Bartkowiak, J. H. Park, J. Y. Lee, J. Y. Kim, N. H. Sung, B. K. Cho, C. U. Jung, J. S. Kim, and H. J. Lee, Phys. Rev. B **80**, 144512 (2009).

[13] M. Kano, Y. Kohama, D. Graf, F. Balakirev, A. S. Sefat, M. A. McGuire, B. C. Sales, D. Mandrus, and S. W. Tozer, J. Phys. Soc. Jpn. **78**, 084719 (2009).

[14] M. M. Altarawneh, K. Collar, C. H. Mielke, N. Ni, S. L. Bud'ko, and P. C. Canfield, Phys. Rev. B **78**, 220505(R) (2008).

[15] N. Ni, M. E. Tillman, J.-Q. Yan, A. Kracher, S. T. Hannahs, S. L. Bud'ko, and P. C. Canfield, Phys. Rev. B **78**, 214515 (2008).

[16] S. Khim, J. W. Kim, E. S. Choi, Y. Bang, M. Nohara, H. Takagi, and K. H. Kim, Phys. Rev. B **81**, 184511 (2010).

[17] E. D. Mun, M. M. Altarawneh, C. H. Mielke, V. S. Zapf, R. Hu, S. L. Bud'ko, and P. C. Canfield, Phys. Rev. B **83**, 100514(R) (2011).

[18] K. Cho, H. Kim, M. A. Tanatar, Y. J. Song, Y. S. Kwon, W. A. Coniglio, C. C. Agosta, A. Gurevich, and R. Prozorov, Phys. Rev. B **83**, 060502(R) (2011).

[19] H. Eschrig and K. Koepernik, Phys. Rev. B **80**, 104503 (2009).

[20] J. Paglione and R. L. Greene, Nat. Phys. **6**, 645 (2010).

[21] S. Weyeneth, R. Puzniak, N. D. Zhigadlo, S. Katrych, Z. Bukowski, J. Karpinski, and H. Keller, J. Supercond. Novel Magnetism **22**, 347 (2009).

[22] A. Gurevich, Phys. Rev. B **67**, 184515 (2003).

[23] M. M. Altarawneh, C. H. Mielke, and J. S. Brooks, Rev. Sci. Instrum. **80**, 066104 (2009).

[24] C. Mielke, J. Singleton, M.-S. Nam, N. Harrison, C. C. Agosta, B. Fravel, and L. K. Montgomery, J. Phys.: Condens. Matter **13**, 8325 (2001).

[25] T. Coffey, Z. Bayindir, J. F. DeCarolis, M. Bennett, G. Esper, and C. C. Agosta, Rev. Sci. Instrum. **71**, 4600 (2000).

[26] V. G. Kogan and R. Prozorov, e-print arXiv:1112.0996.

[27] N. R. Werthamer, E. Helfand, and P. C. Hohemberg, Phys. Rev. **147**, 295 (1966).

[28] A. M. Clogston, Phys. Rev. Lett. **9**, 266 (1962).

[29] K. Maki, Phys. Rev. **148**, 362 (1966).